Characterization of moment-rotation response of cold-formed steel beams

D. Ayhan[1], B.W. Schafer[2]

Abstract

The objective of this study is to provide a prediction method for characterizing the complete moment-rotation (M-θ) response of cold-formed steel (CFS) members in bending. The work is an ancillary effort related to the National Science Foundation funded Network for Earthquake Engineering Simulation (NEES) project: CFS-NEES (www.ce.jhu.edu/bschafer/cfsnees). The goal of CFS-NEES is to enable performance-based seismic design for cold-formed steel framed buildings. A basic building block of performance-based seismic design is nonlinear structural analysis. For cold-formed steel members, which suffer from local and distortional buckling, existing codes provide peak strength and approximations for stiffness loss prior to peak strength, but no estimation of post-peak M-θ behavior. Complete M-θ response is necessary for nonlinear structural analysis of CFS framed buildings. In this research, existing data, obtained by experiments and finite element analysis, are processed to examine the complete M-θ response in cold-formed steel beams. Using a modification of the simplified model introduced in ASCE 41 for pushover analysis, the M-θ response is parameterized into a simple multi-linear curve. The parameters include the initial stiffness, fully effective limit, reduced pre-peak stiffness, peak moment, post-peak plateau, and post-peak rotation at 50% of the peak moment. It is shown herein that the parameters of this multi-linear M-θ curve may themselves be readily predicted as a function of either the local slenderness or distortional slenderness of the cross-section, as appropriate. Accuracy of the proposed M-θ approximation is assessed. The impact of utilizing the full M-θ response in a single and multi-span CFS beam is demonstrated. The proposed prediction method for M-θ provides a necessary step in the development of nonlinear structural analysis of CFS systems.

1. Introduction

Cold formed steel (CFS) enjoys a wide and growing base of application in civil structures. Although design codes provide full guidance for strength prediction and partial guidance for stiffness of CFS members, member ductility and post-peak response is not addressed.

Collapse analysis of a CFS building system (i.e. a building comprised of load bearing cold-formed steel framing), whether for static loads, wind loads, progressive collapse, or seismic design is predicated on knowledge of the nonlinear response of the components and connections

---

[1] Graduate Research Assistant, Istanbul Technical University, <ayhan@itu.edu.tr>
[2] Professor and Chair, Johns Hopkins University, <schafer@jhu.edu>

that make up a building. Simple determination of the force or moment redistribution in a CFS building system after one member fails may not be accurately completed with current knowledge, requiring current design to ignore system effects and instead concentrate on first member failure. Given that CFS cross-sections are typically locally slender they have a more complicated and less forgiving moment-rotation response than compact hot-rolled steel beams. Therefore, simple elastic-perfectly plastic response as commonly used in steel analysis is not typically appropriate for CFS members.

Further, since much of the nonlinear response in CFS building systems is typically related to the shear walls, CFS member response has not been pursued in much detail. Regardless, this lack of understanding has consequences. For example, in CFS seismic design, buildings are detailed with the goal of concentrating all nonlinear response in pre-tested shearwalls. The capacity of other members (or connections) to absorb any of the deformation (energy) is ignored – as is the potential for redistribution of forces – leading to model predictions divorced from reality and structural systems that do not achieve full economy.

For modeling collapse, particularly under dynamic (seismic) loads, no current method provides guidance on member ductility of CFS members. Without fundamental information on CFS member ductility system modeling for CFS structures to collapse, or under dynamic loads, is impossible. This paper attempts to take the initial steps toward providing this needed information for CFS beams. Existing experiments and finite element analysis in local and distortional buckling are processed as the basis of this study.

2. Existing data
The experiments of Yu and Schafer (2003, 2006, and 2007) and finite element (FE) analysis results of Shifferaw and Schafer (2010), on local and distortional buckling of CFS beams, are utilized herein as the available moment-rotation response of CFS beams. The tests were performed in 4 point bending with paired CFS beams composed of industry standard lipped channel and lipped zee specimens varying from 92 to 305 mm (3.62 to 12 in.) deep and from 1.09 to 2.46 mm (0.043 to 0.097 in.) thick. The centerline dimensions of seventeen cross-sections from Yu an Schafer (2003, 2006), those having $M_{test}>0.95M_y$, were selected for the FE analysis study. From these centerline dimensions the thickness was varied from 1.37 to 3.42 mm (0.0538 to 0.1345 in.), resulting in 187 different FE models. The modeling focused on CFS sections that can develop inelastic reserve; i.e., sections with a peak bending capacity greater than the moment at first yield (and thus presumably the most favorable post-peak M-θ response).
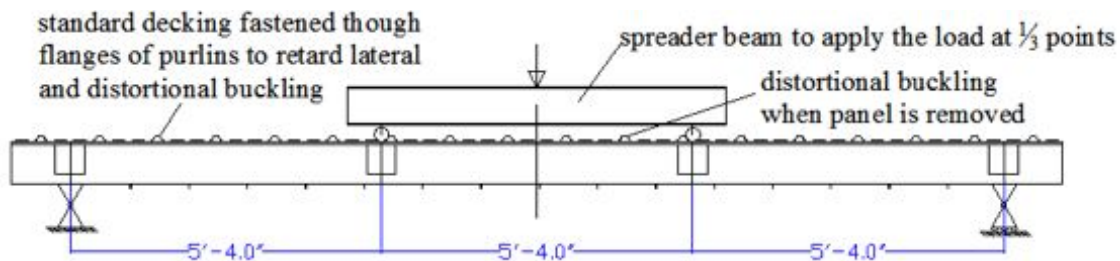

Figure 1: Elevation view of overall test arrangement for four point bending test

The most important parameters in the analysis of the structural behavior of CFS members are the failure mode and the cross-section properties. Therefore, the experimental work realized by Yu

and Schafer (2003, 2006, and 2007) is composed of two test runs carried out on industry standard CFS C and Z-sections. The testing setup (Fig.1) was carefully designed in the first series to allow local buckling failure to form while restricting distortional and lateral-torsional buckling. The corrugated panel attached to the compression flange was removed in the constant moment region in the second tests series so that distortional buckling was then unrestricted.

Shifferaw and Schafer (2010) used the experiments of Yu and Schafer (2003, 2006) to develop and validate an ABAQUS nonlinear collapse shell finite element (FE) model focusing on local and distortional buckling limit states in typical lipped channel and lipped zee CFS sections. The goal of these analyses was not to recreate the tests but rather to provide an idealized model that could consistently provide local and distortional buckling failure modes in a computationally efficient manner. The selected model includes only the central 1.63 m (64 in.) constant moment region from the tests and employs special boundary conditions at the ends and along the flanges.

2.1 Conversion of data
To facilitate the studies herein, the raw data from the tests and FE models were down-sampled to 10 pre-peak points, each one in increments of 10% of the displacement at peak strength.
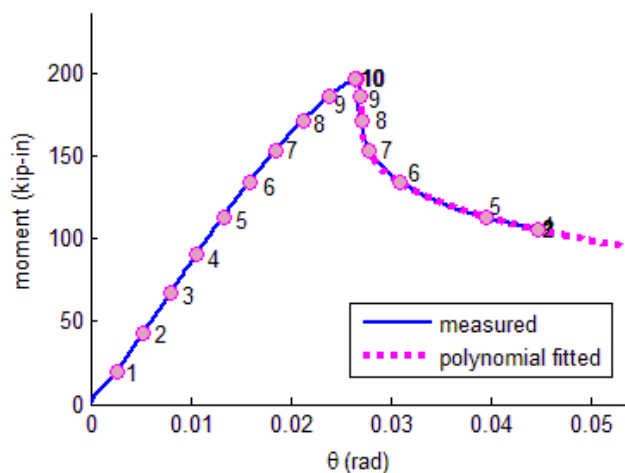
Figure. 2: digitized points (1-10) shown for test 8C068-4E5W
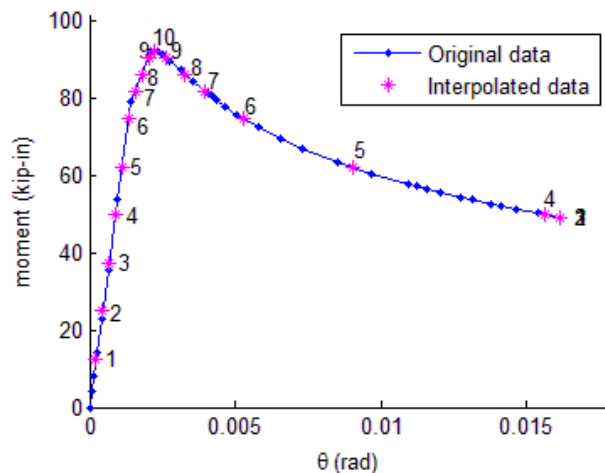
Figure. 3: digitized points (1-10) shown for FE model 8C0685lt11

Based on the force levels corresponding to 10% pre-peak displacement increments, post-peak data was determined. Due to the low density of available data, methods; such as fitting a 3rd order polynomial immediately after the peak strength was completed for the experimental results (*Fig. 2*) while for the finite element analysis results the full curve (*Fig. 3*) was utilized.

2.2 Examination of pre-peak stiffness by available data
The secant stiffness for all available experimental data is calculated and reported in a previous study (Ayhan and Schafer 2011). Secant stiffness values were obtained for the Effective Width Method (EWM) (AISI-S100-07) and Direct Strength Method (DSM) (AISI-S100-07 Appendix 1) and compared against the measured values in Fig. 4. In this figure the horizontal axis is the cross-section slenderness (either local or distortional). As the moment increases the cross-section slenderness increases and the predictive methods proceed from fully effective to partially

3

effective and the stiffness reduces. Neither the EWM nor the DSM method for reducing the stiffness (I_e) follows the same "shape" as the test data as the section stiffness reduces.

(a) local buckling   (b) distortional buckling
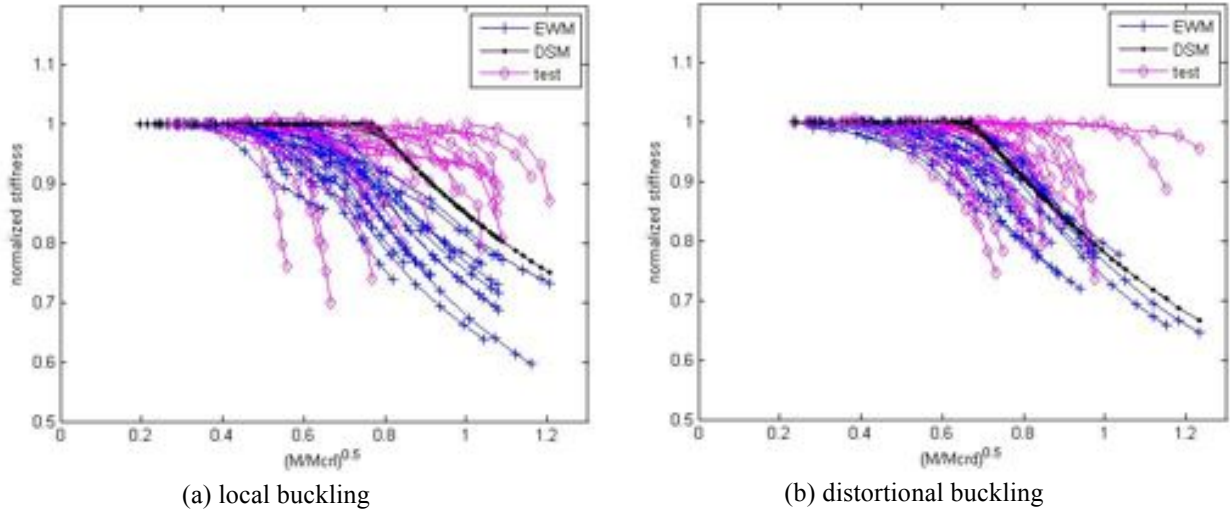
Figure 4: Comparison of DSM and EWM I_{eff} results with (a) local and (b) distortional tests

The EWM provides cross-section specific predictions of the reduced stiffness. The reductions initiate earlier and are more severe than the observed stiffness reductions. The DSM method provides a singular prediction as a function of cross-section slenderness – so all sections reduce stiffness in the same manner. The predicted DSM reductions follow the mean of observed stiffness, but much scatter remains. The EWM reductions generally follow the same shape as the DSM reductions. The DSM reductions provide an upperbound to the EWM reductions.

Table 1: Summary of Test-to-Predicted Ratios for I_{eff} by EWM and DSM

|			$k_{secant-test}/k_{secant-predicted}$ at									
			δ_{peak}	$0.9\delta_{pea}$	$0.5\delta_{pea}$	$0.2\delta_{pea}$	$0.1\delta_{pea}$	δ_{peak}	$0.9\delta_{pea}$	$0.5\delta_{pea}$	$0.2\delta_{pea}$	$0.1\delta_{pea}$
			TESTS					ABAQUS MODELS				
LOCAL		n	24	24	21	9	7	76	76	76	76	76
	DSM	μ	0.97	1.01	0.99	0.99	1.00	0.62	0.68	0.89	0.96	0.98
		CV	0.15	0.13	0.03	0.01	0.00	0.36	0.35	0.23	0.13	0.07
		min	0.70	0.75	0.93	0.98	1.00	0.06	0.07	0.12	0.28	0.54
		max	1.19	1.23	1.06	1.00	1.00	1.12	1.16	1.02	1.00	1.00
	EWM	μ	1.13	1.17	1.07	0.99	1.00	0.61	0.67	0.89	0.96	0.98
		CV	0.18	0.15	0.07	0.01	0.00	0.34	0.33	0.23	0.13	0.07
		min	0.77	0.83	0.98	0.98	1.00	0.06	0.07	0.12	0.28	0.54
		max	1.54	1.55	1.27	1.00	1.00	0.95	1.01	1.00	1.00	1.00
DISTORTIONAL		n	22	22	20	9	7	78	78	78	78	78
	DSM	μ	0.97	1.00	0.98	0.97	1.00	0.68	0.74	0.93	0.98	0.98
		CV	0.21	0.19	0.11	0.04	0.00	0.34	0.32	0.14	0.05	0.07
		min	0.43	0.46	0.62	0.88	1.00	0.13	0.14	0.25	0.60	0.54
		max	1.43	1.42	1.18	1.01	1.00	1.13	1.18	1.01	1.01	1.00
	EWM	μ	1.03	1.06	1.02	0.98	1.00	0.64	0.70	0.92	0.96	0.98
		CV	0.20	0.19	0.11	0.04	0.00	0.29	0.28	0.14	0.13	0.07
		min	0.46	0.50	0.68	0.89	1.00	0.13	0.14	0.25	0.28	0.54
		max	1.48	1.46	1.20	1.02	1.01	0.92	0.98	1.01	1.00	1.00

Note: n=number of tests used, μ=average, CV=coefficient of variation

A statistical summary comparing EWM and DSM to the measured data is provided in Table 1 for both test and FE models. Many of the models fail at strengths greater than the moment at first yield and thus experience stiffness reduction due to yielding, not local or distortional buckling. As a result, only those tests or FE models with capacity less than the moment at first yield are included in the statistical summary of Table 1.

Focusing on the accuracy of the stiffness prediction at peak displacement (δ_{peak}), the statistical summary of Table 1 shows that neither the EWM nor DSM methods provide a highly accurate stiffness prediction method. In comparison with the tests of Yu and Schafer (2003, 2006) the DSM approach is modestly more accurate, and arguably simpler than the EWM. Interestingly, although the EWM provides a cross-section specific stiffness prediction its coefficient of variation is still higher than DSM; thus the scatter is not improved by this additional effort. However, Table 1 shows both methods to be lacking when compared to the FE models; further work is clearly needed.

3. ASCE 41 M-θ definitions

The latest in a series of documents developed to assist engineers with the seismic assessment and rehabilitation of existing buildings (FEMA 273, 1997; FEMA 356, 2000) is ASCE/SEI 41 (2007). These documents provide a comparison of generalized deformation (Δ) and force demands (Q) for different seismic hazards against deformation and force capacities for various performance levels to provide a performance-based seismic engineering framework.
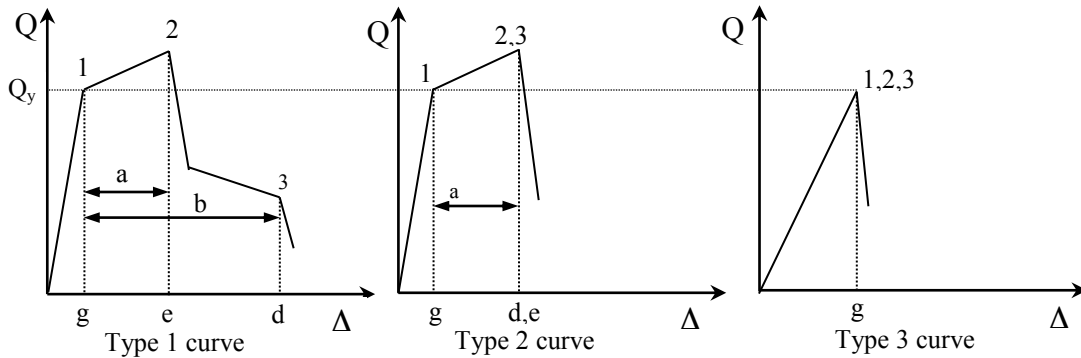
Figure 5: Component force-deformations curves of ASCE 41 (2007)

The ductile performance of steel structures is highly dependent on the ability of its members to dissipate energy by means of hysteretic behavior. The amount of dissipated energy is usually correlated with area under the force-deformation/moment-rotation curve. ASCE/SEI 41 (2007) provides three basic types of component force-deformation curves (Fig. 5, where Q=M and Δ=θ, all parameters are define in ASCE 41). The acceptance criteria for each type are defined depending on the performance level.

ASCE 41 does not include explicit predictions for CFS members; therefore, here ASCE 41 backbone 'curve fitting' exercises are realized for CFS members. An ASCE 41 Type 1 curves assume an elastic range followed by a plastic range including strain hardening, then a post-peak strength degraded range. This is modified for CFS members, which instead have a pre-peak fully effective (elastic) range, pre-peak partially effective range, a peak which is typically less than the yield capacity of the beam, and then a post-peak strength-degraded range.

5

4. Characterization of CFS M-θ with ASCE 41-like models

The area under the moment-rotation curve, which defines the energy dissipated, is one measurement of ductile behavior. Therefore, equating the area under the original curve to the modelled curve is the first aim for the the characterization of the multi-linear moment-rotation models developed here. This was completed in two pieces, pre-peak energy and post-peak energy; so that over/undershooting pre-peak energy is not over/under compensated for in the post-peak range. Besides, the shape of the moment-rotation curve has an important effect on characterization of the ASCE 41-like M-θ models. As Type 1 (Fig. 5) curve includes both pre-peak stiffness loss and post-peak moment degradation features, it was selected as best able to represent the behavior of CFS beams. Accordingly, Model 1, Model 2, and Model 1a (Fig. 6-8) are generated to examine the available data. The test data of Yu and Schafer (2003, 2006) and the FE results of Shifferaw and Schafer (2010) are down-sampled and converted from load-displacement to moment-rotation and then ASCE41-like models are "fit" to the data.

The optimization problem, to define the parameters which are needed to characterize CFS moment-rotation response via the Type 1 curve, is solved in MATLAB. The error considered was calculated as the sum of squares of the difference of pre-peak area under the curves and difference of post-peak area under the curves. The key point in selecting from the three moment-rotation models obtained, are the curve shape and its ability to properly capture the energy.

In the optimization the model parameters are defined as matrix p as follows (see Fig. 9 – 11)

$$p = [M_1 \ k_1 \ M_2 \ k_2 \ \Delta\theta \ \Delta M \ \theta_4] \tag{1}$$

where M_1 is the elastic moment, k_1 is the elastic stiffness, M_2 is the peak moment, k_2 is the second stiffness between elastic and the peak point, $\Delta\theta$ is the rotation step after the peak point and ΔM is the moment drop after the peak point, and θ_4 is the maximum rotation where the modeled M-θ curve terminates. The rotations are defined by the selected model parameters as follows:

$$\theta_1 = \frac{M_1}{k_1} \tag{2}$$

$$\theta_2 = \theta_1 + \frac{M_2 - M_1}{k_2} \tag{3}$$

$$\theta_3 = \theta_2 + \Delta\theta \tag{4}$$

The parameters are constrained in the error minimization as $\theta_1 > 0$, $\theta_1 < \theta_2 < \theta_3 < \theta_4$ and $M_1 > 0$, $M_2 > M_1$, $M_3 < M_2$, $M_3 > 0$.

The 'fit' is sensitive to initial conditions. Ultimately, the initial conditions constrained the model such that the initial stiffness, peak moment, and maximum rotation match the available data exactly. The initial conditions are as follows:

$$M_{1i} = 0.9\max(M_t) \tag{5}$$

$$k_{1i} = k_t \text{ (evaluated at } 50\%M_{t\text{-prepeak}}) \tag{6}$$

$$M_{2i} = \max(M_t) \tag{7}$$

$$k_{2i} = (M_{2i} - M_{1i})/(\theta_{2i} - M_{1i}/k_{1i}) \tag{8}$$

$$\Delta\theta_i = (\theta_t \text{ (at } 0.8M_{t\text{-postpeak}}) - \theta_t \text{ (at } \max(M_t)) \geq 0) \tag{9}$$

$$\Delta M_i = \max(M_t) - \min(M_{t\text{-postpeak}}) \text{ or } 0.5\max(M_t) \tag{10}$$

$$\theta_{4i} = \max(\theta_t) \text{ or } \theta_t \text{ (at } 0.5M_{t\text{-postpeak}}) \tag{11}$$

where the subscript "t" denotes 'test' and "i" an 'initial' guess in the optimization.

4.1 Model 1: post-peak plateau and strength drop
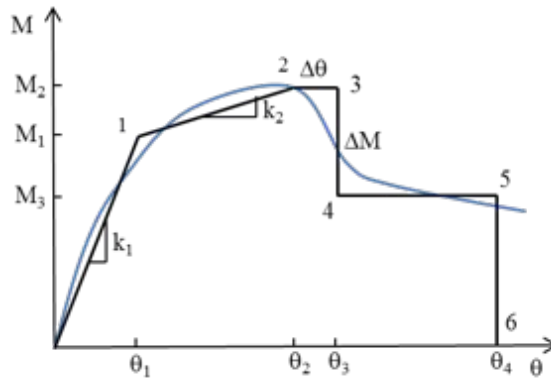
Figure 6: Model 1 backbone curve

Table 2: Variables defining M-θ curve of Model 1

point no	rotation	moment	stiffness	parameters selected
1	θ_1	M_1	k_1	M_1, k_1
2	θ_2	M_2	k_2	M_2, k_2
3	$\theta_3, \Delta\theta$	M_2	0	$\Delta\theta$
4	$\theta_3, \Delta\theta$	$M_3, \Delta M$	∞	$\Delta\theta, \Delta M$
5	θ_4	$M_3, \Delta M$	0	$\theta_4, \Delta M$
6	θ_4	0	∞	θ_4

Model 1 includes pre-peak stiffness loss and a post-peak moment degradation which is described as a combination of post-peak plateau and strength drop (Fig. 6). This shape is defined with 6 points, see Table 2. Parameters which are necessary to characterize this model were selected and used to solve the optimization problem.

4.2 Model 2: post-peak plateau and stiffness loss

The shape of Model 2 is differentiated from Model 1 by the post-peak moment degradation. The post-peak region employs a post-peak plateau and stiffness loss (Fig. 7). The aim is to reflect real behavior of CFS beams. This curve is composed of five critical points, which are defined in Table 3.
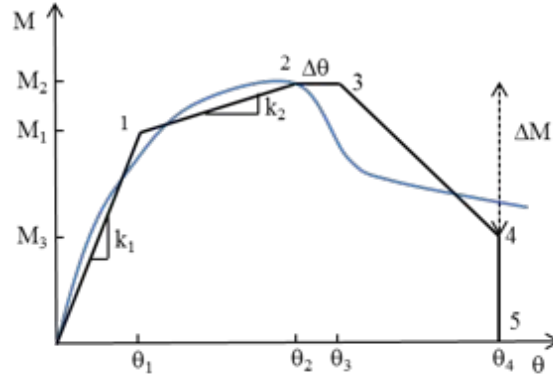

Figure 7: Model 2 backbone curve

Table 3: Variables defining M-θ curve of Model 2

point no	rotation	moment	stiffness	parameters selected
1	θ_1	M_1	k_1	M_1, k_1
2	θ_2	M_2	k_2	M_2, k_2
3	$\theta_3, \Delta\theta$	M_2	0	$\Delta\theta$
4	θ_4	$M_3, \Delta M$	k_3	$\theta_4, \Delta M$
5	θ_4	0	∞	θ_4

4.3 Model 1a: post-peak bilinear stiffness loss

The post-peak strength loss is composed of a bilinear stiffness loss curve in Model 1a (Fig. 8). The critical points to define this shape are given Table 4. An additional parameter (M_4) is needed to characterize Model 1a. The vector of controlling parameters is revised as following:

$$p = [M_1 \; k_1 \; M_2 \; k_2 \; \Delta\theta \; \Delta M \; \theta_4 \; M_4] \tag{12}$$
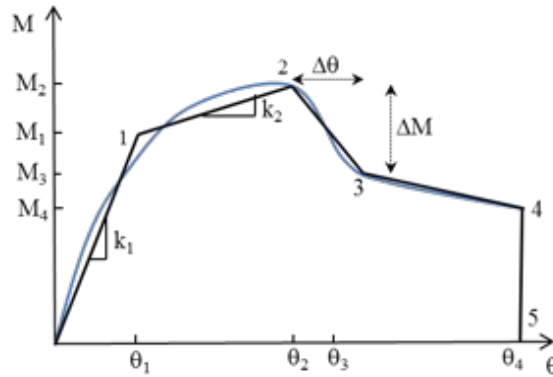

Figure 8: Model 1a backbone curve

Accordingly, a constraint of $M_3 > M_4 > 0$ is added and initial conditions are modified with the following:

$$\Delta\theta_i = (\theta_{4i} - \theta_{2i})/2 \tag{13}$$

$$\Delta M_i = (M_t(at\ \theta_{4i}) - max(Mt))/2 \tag{14}$$

Table 4: Variables defining M-θ curve of Model 1a

point no	rotation	moment	stiffness	parameters selected
1	θ_1	M_1	k_1	M_1, k_1
2	θ_2	M_2	k_2	M_2, k_2
3	$\theta_3, \Delta\theta$	$M_3, \Delta M$	k_3	$\Delta\theta, \Delta M$
4	θ_4	M_4	k_4	θ_4, M_4
5	θ_4	0	∞	θ_4

4.2.4 Characterization of results and recommendation

The multi-linear ASCE 41-like models (Model 1, Model2, Model 1a) were fit separately to the down-sampled data generated from the tests of Yu and Schafer (2003 and 2006) and the FE models of Shifferaw and Schafer (2010). Several "fits" were pursued, four are detailed here. Two of the "fits" use all available data and the others limit the data to only $M_{postpeak} > 50\% M_{t\text{-}postpeak}$. For both, "fits" are realized by either minimizing sum squared error on all 7 model parameters termed the "full fit", or by fitting only k_2, $\Delta\theta$, and ΔM termed the "const. fit". The constrained fit (abbreviated "const. fit") constrains the initial stiffness (k_1) and the peak (θ_2, M_2) as well as the final moment (M_4) to be the same as the test, also only in Model 1a final rotation (θ_4) is also fixed to be the same as the test in the "const. fit".

Typical fitted M-θ of Model 1, Model 2 and Model 1a for local and distortional buckling test data of Yu and Schafer (2003, 2006) are realized and results for test 8C068-4E5W (Yu and Schafer 2003), termed L11 here is provided in Fig. 9. Although all models equate pre- and post-peak energy accurately, Model 1a and Model 2 do not fit the observed post-peak M-θ response for either the local or distortional buckling test data of Yu and Schafer. Model 1 provides the best efficiency for equating both the M-θ shape and the energy dissipated to produce general design expressions.

Even if Model 1a seems to provide more reliable characterization of M-θ behavior for the four point bending tests and simulations, there is no suitable way to predict M_4, the post-peak moment capacity of Model 1a. Model 1 gives more applicable results as error residuals are reasonable (generally less than 1×10^{-10}) and M-θ backbone follows a similar path to the available data. Therefore adaptation of Model 1 is recommended.
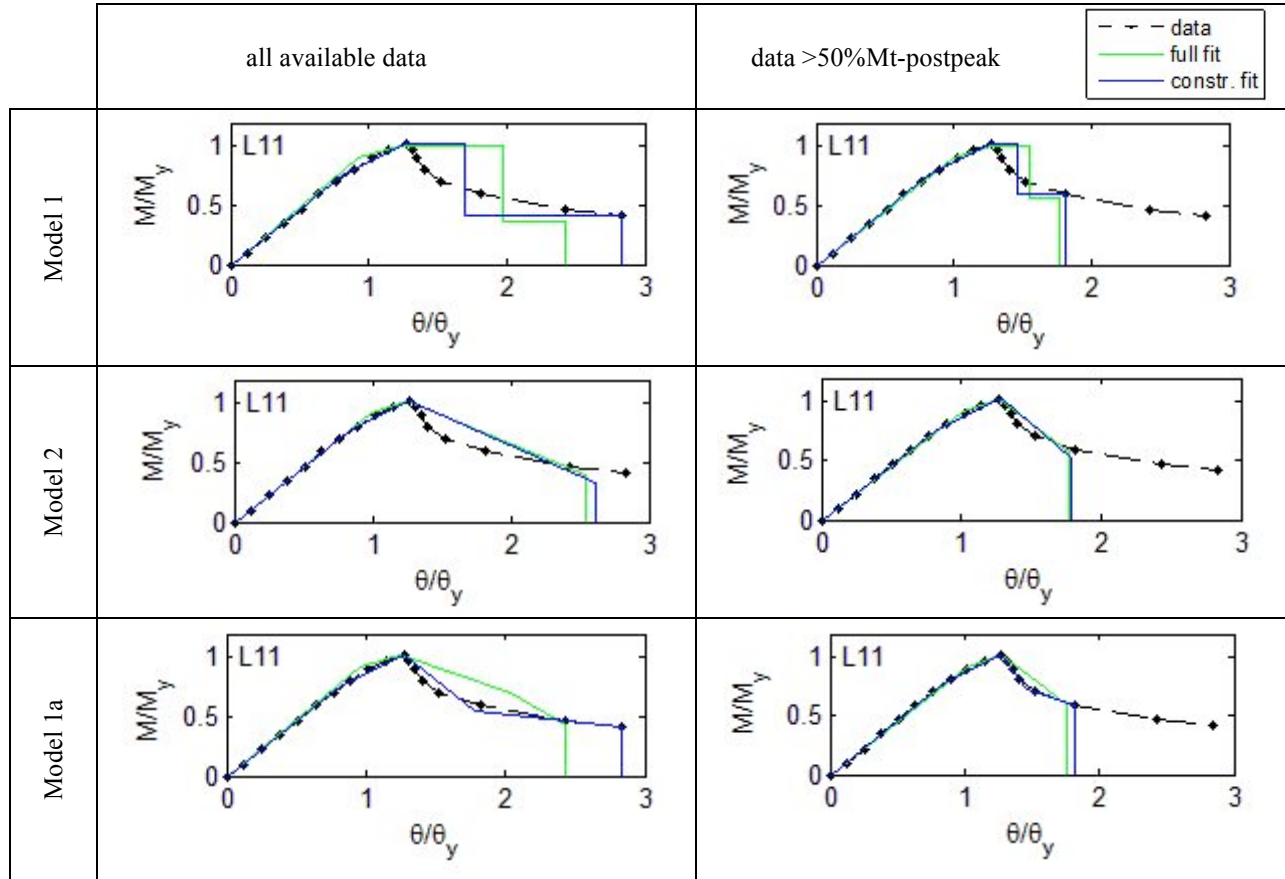
Figure 9: Typical fits for local buckling test result of 8C068-4E5W

5. Design parameterization and prediction for CFS-NEES: Model1

A systematic design method for predicting the parameters of the M-θ backbone curve, applicable to all CFS beams failing in either local or distortional buckling is needed. The Model 1 (Fig. 6) "const. fit" with the data limited to $M_{postpeak}$ >50%$M_{t\text{-}postpeak}$ is employed for the parameterization conducted here. The objective is to create functional relationships that predict the Model 1 parameters, as predicted in the preceding optimization.

5.1 Local buckling

Due to the large range of observed M-θ behavior it is not possible to provide fixed values for the Model 1 parameters as is typical, for example, in ASCE 41. However, existing design does provide insights on how to predict many of the Model 1 parameters. For example, the peak moment capacity (M_2), is known to be well predicted by the Direct Strength Method (DSM) of AISI-S100. DSM uses local cross-section slenderness (λ_ℓ) as the key variable for predicting strength, where:

$$\lambda_\ell = \sqrt{\frac{M_y}{M_{cr\ell}}} \tag{15}$$

10

M_y is the elastic yield moment, and $M_{cr\ell}$ is the elastic critical local buckling moment. Specifically, if the peak moment M_2 is set to $M_{n\ell}$ in the existing DSM provisions, then

$$\frac{M_2}{M_y} = \begin{cases} 1 + \left(1 - \dfrac{1}{C_{yl}^2}\right)\dfrac{\left(M_p - M_y\right)}{M_y} & and \quad C_{yl} = \sqrt{\dfrac{0.776}{\lambda_l}} \leq 3 \quad if \quad \lambda_l < 0.776 \\[4mm] \left(1 - 0.15\left(\dfrac{1}{\lambda_l^2}\right)^{0.4}\right)\left(\dfrac{1}{\lambda_l^2}\right)^{0.4} & if \quad \lambda_l > 0.776 \end{cases}$$ (16)
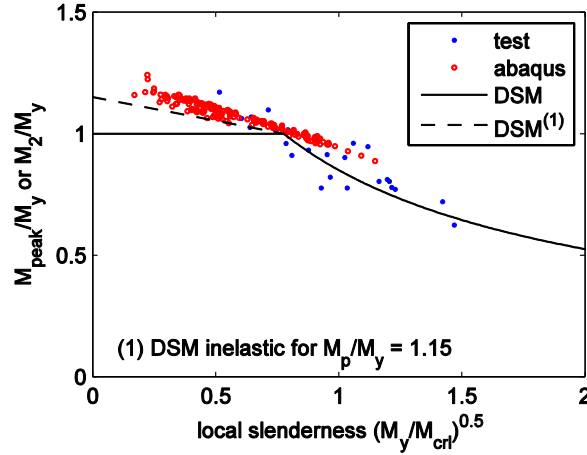

Figure 10: Peak moment strength as a function of local slenderness

Note, the provisions for $\lambda_\ell < 0.776$ were adopted in AISI-S100 in February 2011 based on the work of Shifferaw and Schafer (2010). Performance of these expressions against the available data is provided in Fig. 10. Schafer (2008) provides additional discussion and validation of the DSM approach.

A key parameter for CFS beams in Model 1 is the rotation at the peak moment (M_2). It is known that locally slender cross-sections have a reduced stiffness so the rotation at peak (θ_2) can be significantly larger than the elastic rotation (i.e. M_2/k_1 where k_1 is the initial elastic stiffness, also known as k_e). Fig. 11 provides θ_2 normalized by the yield rotation θ_y ($\theta_y = M_y/k_1$ or M_y/k_e) as a function of local slenderness. Somewhat remarkably, the available data exhibits a clear trend with local slenderness and a simple expression is proposed as shown in the figure:

$$\frac{\theta_2}{\theta_y} = \frac{1}{\lambda_\ell}$$ (16)

This simple expression provides a means to determine the reduced stiffness that occurs due to local buckling, unlike existing stiffness predictions (Section 3) this stiffness method is decoupled from the strength prediction.
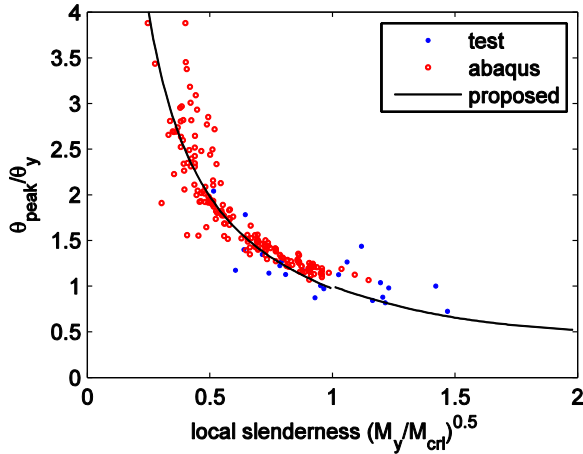
Figure 11: Peak rotation ($\theta_{peak}=\theta_2$) as a function of local slenderness
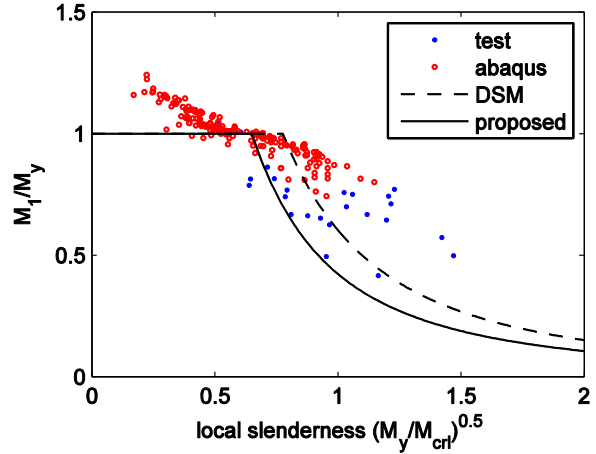
Figure 12: "Fully effective" moment (M_1) as a function of local slenderness

With the peak point anchored the development of the design method may now turn to other Model 1 parameters. Specifically, the pre-peak behavior must be completed, by determining either M_1 or θ_1 – it is assumed k_1 (the elastic stiffness) is known. It is typical in current CFS beam design to determine the moment at which a section becomes "partially effective", for Model 1, this moment is M_1. Therefore, M_1 is explored directly here, as shown in Fig. 12.

The scatter in prediction of M_1 (Fig. 12) is greater than for M_2 (Fig. 11). Nonetheless, the trend with respect to local slenderness remains. A simple expression is fit to the data:

$$\frac{M_1}{M_y} = \left\{ \begin{array}{ll} 1 & \text{if } \lambda_\ell < 0.650 \\ \left(\dfrac{0.650}{\lambda_\ell}\right)^2 & \text{if } \lambda_\ell \geq 0.650 \end{array} \right\} \leq \frac{M_2}{M_y} \tag{17}$$

The proposed relation between M_1 and local slenderness is a departure from current practice because (a) it disconnects the stiffness prediction from the strength prediction, and (b) it implies that the local slenderness (λ_ℓ) must be as small as 0.650 for the section to be fully effective. Current design assumes that when the strength reaches M_y (i.e., $\lambda_\ell = 0.776$) the section is fully effective. In the proposed expressions a CFS beam must exhibit moderate inelastic reserve capacity if it is to be fully effective (elastic) up to its peak moment.

The post-peak performance has greater scatter in the observed data than the peak and pre-peak behavior. Fig. 13 provides θ_4 for the available data versus local slenderness as proposed below:

$$\frac{\theta_4}{\theta_y} = \left\{ \begin{array}{ll} 1.5\dfrac{1}{\lambda_\ell} & \text{if } \lambda_\ell > 1 \\ 1.5\left(\dfrac{1}{\lambda_\ell}\right)^{1/4\lambda_\ell} & \text{if } \lambda_\ell \leq 1 \end{array} \right\} \tag{18}$$

a) for limeted number   b) for all data
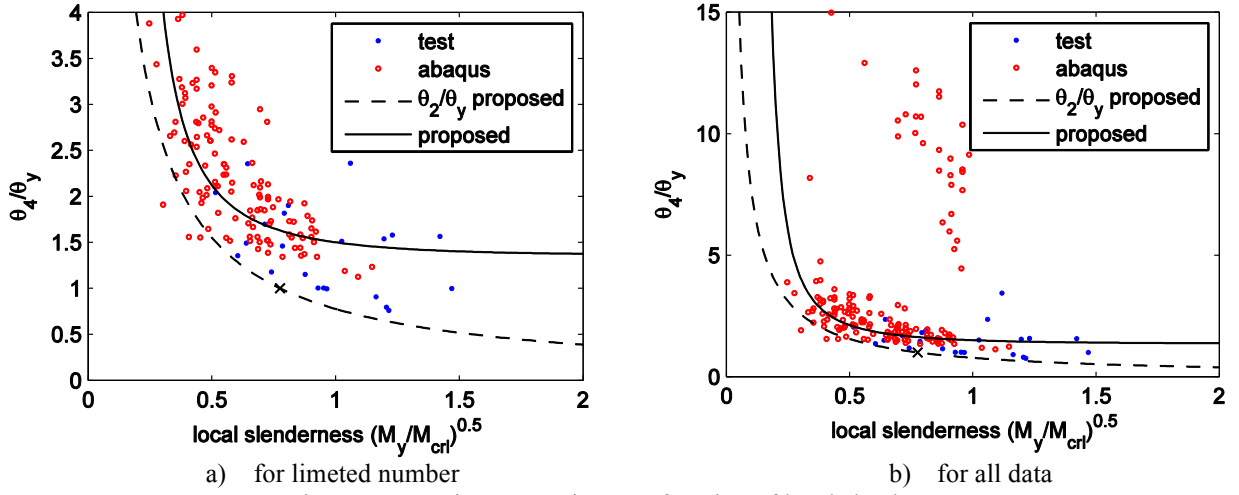
Figure 13: Maximum rotation as a function of local slenderness

Finally, this leaves the post-peak parameters $\Delta\theta$ and ΔM in need of prediction expressions. In general $\Delta\theta$ is intended to capture post-peak yielding; theoretically this is only significant for sections with inelastic reserve. Fig. 14 provides the post-peak yielding $\Delta\theta$ as a function of local slenderness for the available data.
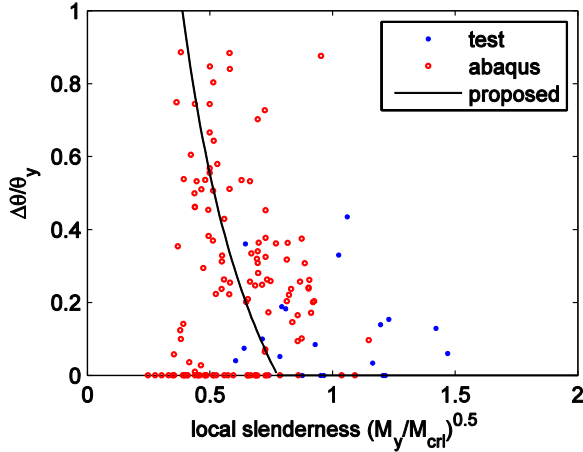

Figure 14: Post-peak yielding ($\Delta\theta$) as a function of local slenderness
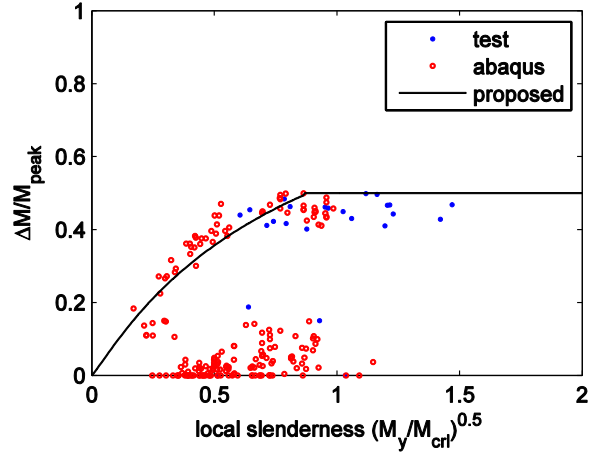
Figure 15: Post-peak moment drop (ΔM) as a function of local slenderness (note $M_{peak}=M_2$)

The scatter is large in Fig. 14 and many sections that have strength below M_y exhibit some post-peak yielding. However, for simplicity it is proposed that only sections with strength greater than M_y be predicted to have nonzero $\Delta\theta$. The following expressions are proposed for use and shown in Fig. 14:

$$\frac{\Delta\theta}{\theta_y} = \begin{cases} \left(\dfrac{0.776}{\lambda_\ell}\right) - 1 & \text{if } \lambda_\ell < 0.776 \\ 0 & \text{if } \lambda_\ell \geq 0.776 \end{cases} \tag{19}$$

Table 5: Design expressions for local buckling

	Local
	$\lambda_\ell = \sqrt{\dfrac{M_y}{M_{cr\ell}}}$
rotations	$\dfrac{\theta_1}{\theta_y} = \dfrac{M_1}{k_1 \theta_y} = \dfrac{M_1}{k_e \theta_y} = \dfrac{M_1}{M_y}$ (note, M_1 given below)
	$\dfrac{\theta_2}{\theta_y} = \dfrac{1}{\lambda_\ell} \leq \dfrac{M_2}{k_e}$
	$\theta_3 = \theta_2 + \Delta\theta$, where $\Delta\theta$ is: $$\dfrac{\Delta\theta}{\theta_y} = \begin{cases} \left(\dfrac{0.776}{\lambda_\ell}\right) - 1 & \text{if } \lambda_\ell < 0.776 \\ 0 & \text{if } \lambda_\ell \geq 0.776 \end{cases}$$
	$$\dfrac{\theta_4}{\theta_y} = \begin{cases} 1.5\dfrac{1}{\lambda_\ell} & \text{if } \lambda_\ell > 1 \\ 1.5\left(\dfrac{1}{\lambda_\ell}\right)^{1/4\lambda_\ell} & \text{if } \lambda_\ell \leq 1 \end{cases}$$
moments	$$\dfrac{M_1}{M_y} = \begin{cases} 1 & \text{if } \lambda_\ell < 0.650 \\ \left(\dfrac{0.650}{\lambda_\ell}\right)^2 & \text{if } \lambda_\ell \geq 0.650 \end{cases} \leq \dfrac{M_2}{M_y}$$
	$\dfrac{M_2}{M_y} = \dfrac{M_{n\ell}}{M_y}$ where $M_{n\ell}$ is per AISI-S100, i.e.: $$\dfrac{M_2}{M_y} = \begin{cases} 1 + \left(1 - \dfrac{1}{C_{y\ell}^2}\right)\dfrac{(M_p - M_y)}{M_y} \text{ and } C_{y\ell} = \sqrt{\dfrac{0.776}{\lambda_\ell}} \leq 3 & \text{if } \lambda_\ell < 0.776 \\ \left(1 - 0.15\left(\dfrac{1}{\lambda_\ell^2}\right)^{0.4}\right)\left(\dfrac{1}{\lambda_\ell^2}\right)^{0.4} & \text{if } \lambda_\ell \geq 0.776 \end{cases}$$
	$M_3 = M_2 - \Delta M$, where ΔM is: $\dfrac{\Delta M}{M_2} = 1 - 1/\left(\dfrac{\lambda_\ell}{0.776} + 1\right)^{1.1} \leq 0.5$

Ancillary expressions useful for defining the complete curve include

$$k_2 = \dfrac{M_2 - M_1}{\theta_2 - \theta_1}$$

Finally, the post-peak moment drop (ΔM) is explored. Note (Δθ,ΔM) + (θ₂,M₂) = (θ₃,M₃), so determination of ΔM is the final necessary parameter for Model 1. The post-peak moment drop is provided as a function of local slenderness for the available data in Fig. 15. For some of the data little or no moment drop is observed, this occurs in models where sufficient post-peak rotation was not explored (either the test or the FE model was stopped before reaching high post-peak rotations). Thus, the data with post-peak moment drop is the most important. In the absence of a definitive theory it is presumed that a 50% moment drop exists for all sections with some local buckling strength reduction ($\lambda_\ell > 0.776$) otherwise the moment drop increases from zero as the local slenderness increases via:

$$\frac{\Delta M}{M_2} = 1 - 1 / \left(\frac{\lambda_\ell}{0.776} + 1 \right)^{1.1} \le 0.5 \qquad (20)$$

Taken together the prediction method for developing the CFS-NEES Model 1 backbone curve in local buckling is provided in Table 5.

5.2 Distortional buckling
Distortional buckling is evaluated in the same manner as local buckling and similar design expressions are arrived at. Fig. 16 provides the same information as Figures 10-15 for local buckling. Table 6 provides a summary of the proposed design expressions and Table 7 summarizes the quantitative performance of both the local and distortional buckling method.

Fig. 16(a) indicates that DSM maybe employed to predict the peak strength. Fig. 16(b) shows again that the rotation at the peak moment may be readily predicted as a function of cross-section (distortional in this case) slenderness. The rotation at peak moment (θ_2) in the distortional buckling data (Fig. 16b) is slightly greater than the local buckling data (Fig. 11), so the proposed expression (see Table 6) reflects this. The notion that distortional buckling modes experience greater stiffness reductions than local buckling failures is not commonly recognized in the literature. The fully effective moment, M_1, Fig. 20(c), exhibits significant scatter and similar to the local buckling case (Fig. 12) a convenient expression that generally provides an M_1 slightly below M_2 is selected as shown in Fig. 20(c) and reported in Table 6.

The post-peak Model 1 parameters are captured in Figure 16(d-f) and are arrived at in a similar fashion to the local buckling results. The maximum rotation (θ_4, Fig. 16(d)) is set equal to 1.5 times the rotation at peak moment (θ_2) when $\lambda_d > 1$, exactly the same as in the local buckling case. The inelastic plateau (Δθ, Fig. 16(e)) is only allowed for members predicted to have strength greater than M_y, and otherwise follows that available data as closely as possible. The moment drop expression (ΔM, Fig. 20(f)) follows the same basic expression as local buckling and assumes a 50% drop in moment for sections which experience any reduction in strength due to distortional buckling (i.e., $M_{nd} < M_y$, $\lambda_d > 0.673$).

Overall the quantitative performance of the method is summarized in Table 6. In general the approach is a more conservative predictor than for local buckling, but provides an appropriate method for design.

15
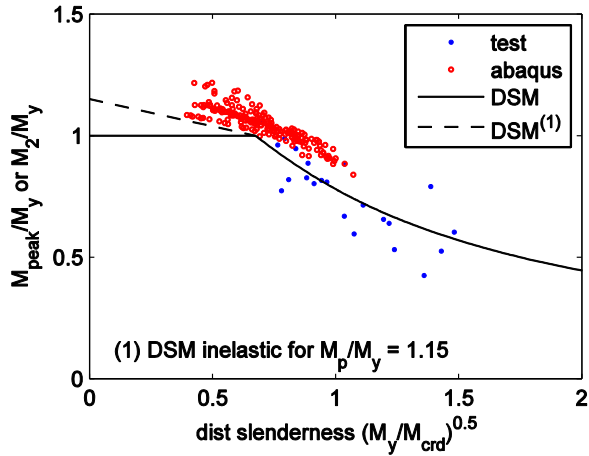
(a) peak moment (M_{peak} or M_2)
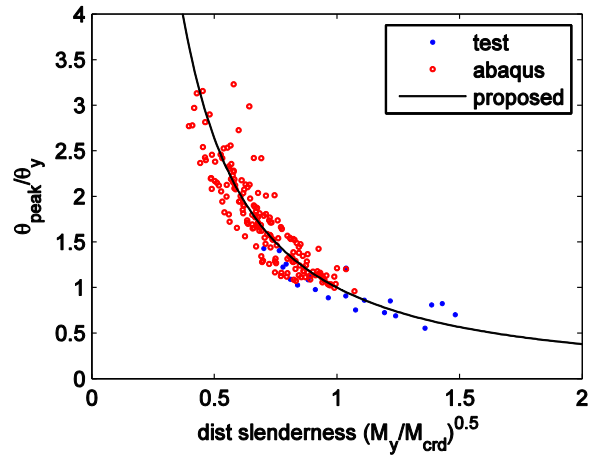
(b) rotation at M_2 (θ_{peak} or θ_2)
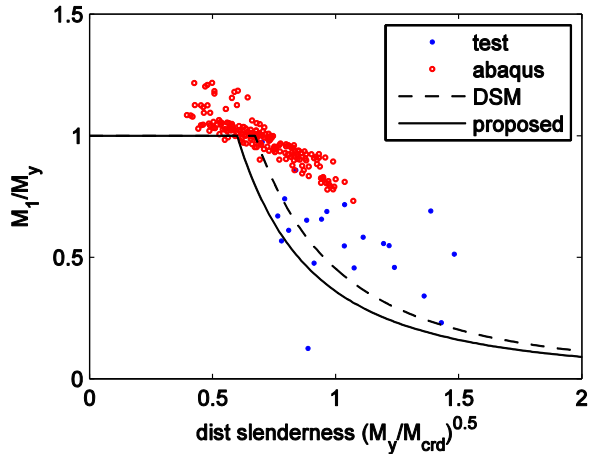
(c) fully effective moment (M_1)
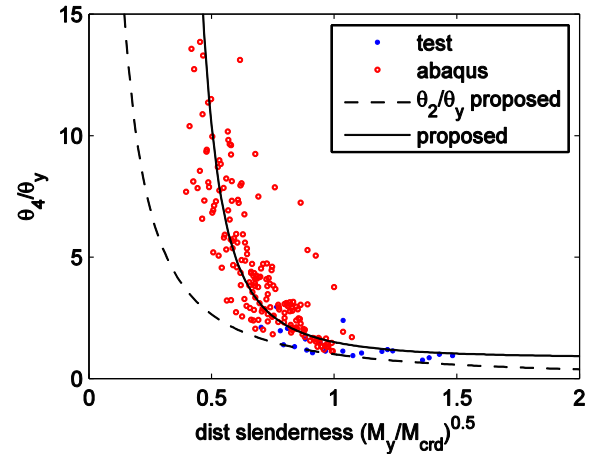
(d) maximum rotation (θ_4)
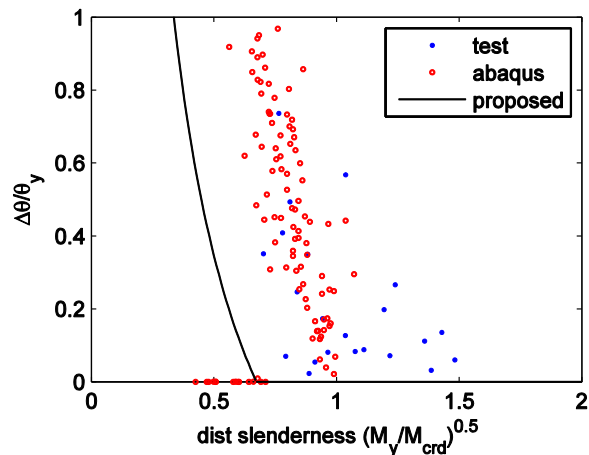
(e) inelastic plateau ($\Delta\theta$)
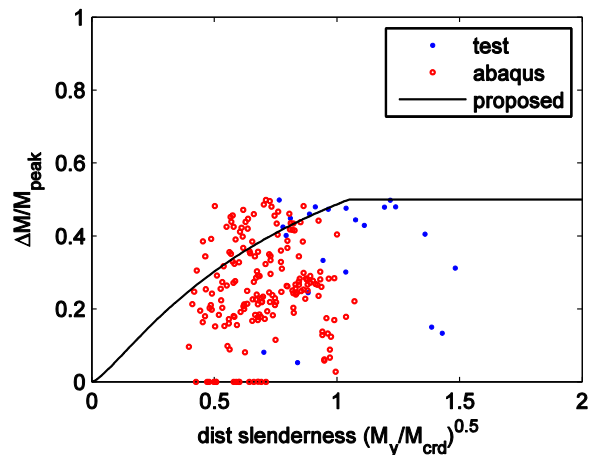
(f) post-peak moment drop (ΔM)

Figure 16: CFS-NEES Model 1a parmaters for available data as a function of distortional slenderness, proposed design expressions indicated by solid lines

Table 6: Design expressions for distortional buckling

	Distortional
	$\lambda_d = \sqrt{\dfrac{M_y}{M_{crd}}}$
rotations	$\dfrac{\theta_1}{\theta_y} = \dfrac{M_1}{k_1\theta_y} = \dfrac{M_1}{k_e\theta_y} = \dfrac{M_1}{M_y}$
	$\dfrac{\theta_2}{\theta_y} = \left(\dfrac{1}{\lambda_d}\right)^{1.4}$
	$\theta_3 = \theta_2 + \Delta\theta$, where $\Delta\theta$ is: $\dfrac{\Delta\theta}{\theta_y} = \begin{cases} \left(\dfrac{0.673}{\lambda_d}\right) - 1 & \text{if } \lambda_d < 0.673 \\ 0 & \text{if } \lambda_d \geq 0.673 \end{cases}$
	$\dfrac{\theta_4}{\theta_y} = \begin{cases} 1.5\left(\dfrac{1}{\lambda_d}\right)^{1.4} & \text{if } \lambda_d > 1 \\ 1.5\left(\dfrac{1}{\lambda_d}\right)^{1.4/\lambda_d} & \text{if } \lambda_d \leq 1 \end{cases}$
moments	$\dfrac{M_1}{M_y} = \begin{cases} 1 & \text{if } \lambda_\ell < 0.600 \\ \left(\dfrac{0.600}{\lambda_d}\right)^2 & \text{if } \lambda_\ell \geq 0.600 \end{cases} \leq \dfrac{M_2}{M_y}$
	$\dfrac{M_2}{M_y} = \dfrac{M_{nd}}{M_y}$ where M_{nd} is per AISI-S100, i.e.:
	$\dfrac{M_2}{M_y} = \begin{cases} 1 + \left(1 - \dfrac{1}{C_{yd}^2}\right)\dfrac{\left(M_p - M_y\right)}{M_y} \text{ and } C_{yd} = \sqrt{\dfrac{0.673}{\lambda_d}} \leq 3 & \text{if } \lambda_d < 0.673 \\ \left(1 - 0.22\left(\dfrac{1}{\lambda_\ell^2}\right)^{0.5}\right)\left(\dfrac{1}{\lambda_\ell^2}\right)^{0.5} & \text{if } \lambda_d \geq 0.673 \end{cases}$
	$M_3 = M_2 - \Delta M$, where ΔM is: $\dfrac{\Delta M}{M_2} = 1 - 1/\left(\dfrac{\lambda_d}{0.673} + 1\right)^{1.4} \leq 0.5$

Ancillary expressions useful for defining the complete curve include

$$k_2 = \frac{M_2 - M_1}{\theta_2 - \theta_1}$$

The accuracy of prediction method for M-θ is qualitatively provided in Fig. 10-15 for local buckling and in Fig. 16 for distortional buckling, a quantitative assessment of the accuracy of the prediction method is provided in Table 7. Consistent with the figures variation (standard deviation) can sometimes be significant; however, taken in total the method performs surprisingly well.

Table 7: Test-to-predicted statistics for proposed design method for generating CFSNEES Model 1 backbone curves

			ratio of test (or FE) - to - predicted for							
			Energy		fully eff. limit	eff. k	peak		drop	
			Pre-peak	Post-peak	M_1	k_{sec}	θ_2	M_2	ΔM	for $\Delta M>0.20M2$
local	tests	mean	1.00	1.03	1.36	1.00	1.06	1.03	0.84	0.97
		st. dev.	0.32	0.61	0.13	0.15	0.20	0.08	0.32	0.09
	FE models	mean	1.18	1.09	1.21	1.01	1.06	1.046	0.400	1.07
		st. dev.	0.71	1.06	0.14	0.15	0.20	0.024	0.467	0.10
	all data	mean	1.16	1.08	1.23	1.01	1.06	1.04	0.45	1.06
		st. dev.	0.66	1.01	0.14	0.15	0.20	0.03	0.45	0.10
distortional	tests	mean	0.89	0.84	1.26	1.01	0.98	0.98	0.75	0.86
		st. dev.	0.26	0.41	0.00	0.16	0.16	0.13	0.31	0.21
	FE models	mean	1.10	1.56	1.21	1.08	1.07	1.10	0.73	0.91
		st. dev.	0.55	0.81	0.07	0.19	0.40	0.04	0.37	0.27
	all data	mean	1.08	1.48	1.21	1.08	1.06	1.08	0.73	0.90
		st. dev.	0.52	0.77	0.07	0.19	0.39	0.06	0.37	0.26

Table 8: Comparison of design expressions results with EWM and DSM for pre-peak stiffness

		δ_{peak}	$0.9\delta_{peak}$	$0.8\delta_{peak}$	$0.7\delta_{peak}$	$0.6\delta_{peak}$	$0.5\delta_{peak}$	$0.4\delta_{peak}$	$0.3\delta_{peak}$	$0.2\delta_{peak}$	$0.1\delta_{peak}$
						$k_{secant-measured}/k_{secant-predicted}$ at					
mean	**LOCAL BUCKLING FE models**										
	DSM	0.62	0.68	0.74	0.79	0.84	0.88	0.92	0.95	0.97	1.00
	EWM	0.61	0.67	0.73	0.79	0.84	0.89	0.92	0.95	0.97	1.00
	D.Exp.	0.98	1.03	1.06	1.06	1.03	1.01	1.00	1.01	1.02	1.02
	LOCAL BUCKLING tests										
	DSM	0.97	1.01	1.02	1.02	1.01	0.99	0.98	0.98	0.99	1.00
	EWM	1.13	1.17	1.16	1.15	1.11	1.07	1.03	1.00	0.99	1.00
	D.Exp.	1.00	1.03	1.04	1.02	1.00	0.98	0.98	0.96	0.96	1.00
	DIST BUCKLING FE models										
	DSM	0.71	0.77	0.83	0.88	0.91	0.94	0.96	0.98	0.99	1.00
	EWM	0.65	0.71	0.77	0.83	0.89	0.93	0.96	0.97	0.99	1.00
	D.Exp.	1.07	1.12	1.15	1.15	1.12	1.06	1.01	1.00	1.00	1.00
	DIST BUCKLING tests										
	DSM	0.97	1.00	1.01	1.01	0.99	0.98	0.97	0.96	0.97	1.00
	EWM	1.03	1.06	1.07	1.07	1.04	1.02	0.99	0.99	0.98	1.00
	D.Exp.	1.02	1.05	1.06	1.06	1.03	1.00	0.97	0.97	0.97	1.00

Table 8 provides a comparison of pre-peak stiffness between the traditional methods of Section 4 (EWM and DSM) and the newly proposed characterization, abbreviated as "D.Exp" in the table. The new expressions are simple in form and provide much improved accuracy over the available approaches. These new expressions are recommended for design.

6. Future Work

Significant future work remains, most notably (a) performing additional cyclic testing to verify and expand the proposed design method based on monotonic testing, (b) implementing the proposed expressions in an analysis framework such that ASCE 41 style pushover analysis can be explored in real structures, and (c) developing companion expressions that address moment-curvature instead of moment-rotation to provide a more fundamental set of expressions for implementation in analysis.

7. Conclusions

Knowledge of the moment-rotation (M-θ) response of cold-formed steel beams is fundamental to the success of cold-formed steel structures. Existing monotonic test and finite element data provide a characterization of the backbone M-θ response of cold-formed steel beams failing in local and distortional buckling limit states. Simplified multi-linear models in the spirit of ASCE 41 formulations are fit to existing data by insuring pre-peak and post-peak energy balance is maintained between the model and the original data. The derived model parameters, e.g. the moment at which pre-peak nonlinear stiffness engages (M_1) or the available rotation at a pos-peak moment level 50% of the peak value (θ_4) are then examined to determine if a simple method may be used in their prediction. It is found that local and distortional cross-sectional slenderness are adequate explanatory variables for parameterizing the simplified M-θ model parameters – and simple design expressions are developed for predicting unique M-θ curves for all cold-formed steel cross-sections in local or distortional buckling. The developed expressions are shown to adequately predict the available data and provide an improvement for pre-peak stiffness prediction when compared to existing methods. In addition, for the first time, post-peak predictions of ductility are available for cold-formed steel beams. Much work remains, but the research demonstrates the viability of a significant expansion of the Direct Strength Method philosophies to the prediction of post-peak member behavior and provides a tool for further exploring the nonlinear response of cold-formed steel systems.

References

American Iron and Steel Institute (AISI). (2007). North American Specification for the Design of Cold-Formed Steel Structural Members; and 2007 edition: Commentary on the Specification, Washington, D.C.

American Iron and Steel Institute (AISI). (2007). Supplement 2007 to the North American Specification for the Design of Cold-Formed Steel Structural Members, 2007 edition, Appendix 1, Design of Cold-Formed Steel Structural Members Using Direct Strength Method, Washington, D.C.

American Society of Civil Engineers (ASCE/SEI 41-06). (2007). Seismic Rehabilitation of Existing Buildings, Reston, Virginia

Ayhan, D, Schafer, BW, "Impact of cross-section stability on member stability and ductility", Structural Stability Research Council (AISI), 2011.

Shifferaw, Y., Schafer, B.W. (2011). "Inelastic Bending Capacity of Cold-Formed Steel Members." ASCE, Journal of Structural Engineering.

Schafer, B.W. (2008) "Review: The Direct Strength Method of cold-formed steel member design." *J. Constr. Steel Res.*, 64(7-8), 766-778.

Yu, C., Schafer, B.W. (2003). "Local buckling Test on Cold-Formed Steel Beams." Journal of Structural Engineering. ASCE, 129 (12) 1596-1606.

Yu, C, Schafer, B.W., (2006). "Distortional buckling tests on cold formed steel beams." Journal of Structural Engineering, ASCE, 515-528.